Complex polarization ordering in $PbTiO_3$ nanowires: A first-principles computational study

G. Pilania and R. Ramprasad*
Department of Chemical, Materials, and Biomolecular Engineering, Institute of Materials Science, University of Connecticut, Storrs, Connecticut 06269, USA
(Received 8 June 2010; published 25 October 2010)

Based on parameter-free density-functional-theory calculations, we demonstrate the possibility of nonrectilinear curling vortex electric dipole configurations in $PbTiO_3$ nanowires. We predict that the critical size for the genesis of the vortex polarization instability (with an axial toroidal moment) is 16 Å. We also report previously unknown phase transitions between the nonrectilinear vortex and conventional rectilinear axial polarization configurations mediated by strain and surface terminations. The ability to switch reversibly between the vortex (clockwise/counterclockwise) and axial (positive/negative) polarization states may open up transformative technological possibilities.

DOI: 10.1103/PhysRevB.82.155442 PACS number(s): 77.80.B−, 77.80.Dj, 62.23.Hj, 31.15.A−

I. INTRODUCTION

At low temperatures, an ideal infinite bulk ferroelectric material can, in principle, support a single-domain polarization configuration in which all dipoles align along one direction in a rectilinear fashion. However, the mere presence of a surface gives rise to uncompensated charges due to the termination of electric polarization at the surface. The surface charges thus produced are either quenched by charges supplied from surroundings, e.g., by a metal electrode or by ionic adsorbates (under the "closed-circuit" condition), or, when the charge compensation is inadequate, result in a depolarizing field (under the "open-circuit" condition). In an attempt to eliminate the depolarizing field, the single domain breaks into a random multidomain structure with net zero polarization. The energy penalty caused by the formation of domain walls is compensated by a decrease in the electrostatic interaction energy of the system due to the elimination or reduction in the depolarizing field.[1,2] Still, the polarization pattern within each domain in such a polydomain system maintains a rectilinear configuration.

The situation changes dramatically as one or more dimensions of the ferroelectric system shrinks to the nanoscale, when it becomes progressively more difficult for the system to annihilate the depolarizing fields through splitting into domains.[3–6] Rather, the polarization vector field may change directions from unit cell to unit cell in an attempt to form "closure" or "vortex" domains with zero net polarization (to minimize the electrostatic energy) but nonzero *local* polarization. Closure domains are thus characterized by the existence of nonrectilinear polarization configurations within a region with the moment of the polarization (i.e., the toroidal moment) serving as the order parameter, rather than the polarization itself, much like the ordering of magnetic moments in nanomagnets.[7,8] This situation represents the happy compromise between the system's desire to stay polarized while simultaneously minimizing depolarizing fields at very small length scales.

Such closure domains in nanoscale ferroelectrics have indeed been predicted in the recent past.[9–19] Fig. 1(a), for example, illustrates the preferred polarization configuration in a 48 Å × 48 Å × 48 Å $PbZr_{0.40}Ti_{0.60}O_3$ nanodots terminated by the {001} family of surfaces, predicted using effective Hamiltonian simulations (parameterized using first-principles data).[10] The local polarization vectors (indicated as arrows corresponding to each unit cell) are oriented along the ⟨001⟩ directions, consistent with the preferred directions for ferroelectric distortions in bulk $PbZr_xTi_{1-x}O_3$ for this system. Although direct experimental observations of such vortex states remain elusive, recent efforts based on peizoresponse force microscopy have yielded evidence suggestive of the existence of such polarization ordering in $PbZr_xTi_{1-x}O_3$ nanodots.[16] Fig. 1(b) shows an example of density-functional-theory (DFT) predictions of closure domains in ultrathin $SrRuO_3/BaTiO_3/SrRuO_3$ ferroelectric capacitors.[14] The local dipoles which point along the [001] or $[00\bar{1}]$ directions at the center of the $BaTiO_3$ layer are closed at the first $SrRuO_3$ electrode layer near the electrode-ferroelectric interface yielding closure domains with 90° domain walls. Again, indirect experimental evidence for the existence of such thin film vortex polarization configurations, in terms of "stripe" domains, is indeed available.[19]

In spite of the presence of mounting evidence for the existence of the vortex polarization domains in zero- and two-dimensional ferroelectric nanostructures, such a possibility for one-dimensional ferroelectric nanowires has not been actively considered. We note that only a few studies on this topic based on the first-principles derived effective Hamiltonian approach exist in the literature.[9,11] Owing to negligible depolarizing fields along the nanowire axis, one may expect nanowires to display conventional rectilinear ferroelectric distortions along their axis in order to satisfy their tendency to be polarized. Indeed, such axial polarization has been predicted in $BaTiO_3$ and $PbTiO_3$ nanowires with sizes larger than 12 Å.[20–23] However, if axial polarization is suppressed (e.g., through strain along the nanowire axis or due to appropriate sidewall surface terminations), one may expect lateral (i.e., off-axis) polarization, but the manner in which such lateral polarization may manifest is unclear. The requirement to minimize depolarizing fields along the lateral direction may force the polarization to occur either entirely in nonrectilinear vortex form (with a nonzero axial toroidal moment), or as a combination of vortex polarization and reduced net nonzero lateral polarization. We note that nonzero

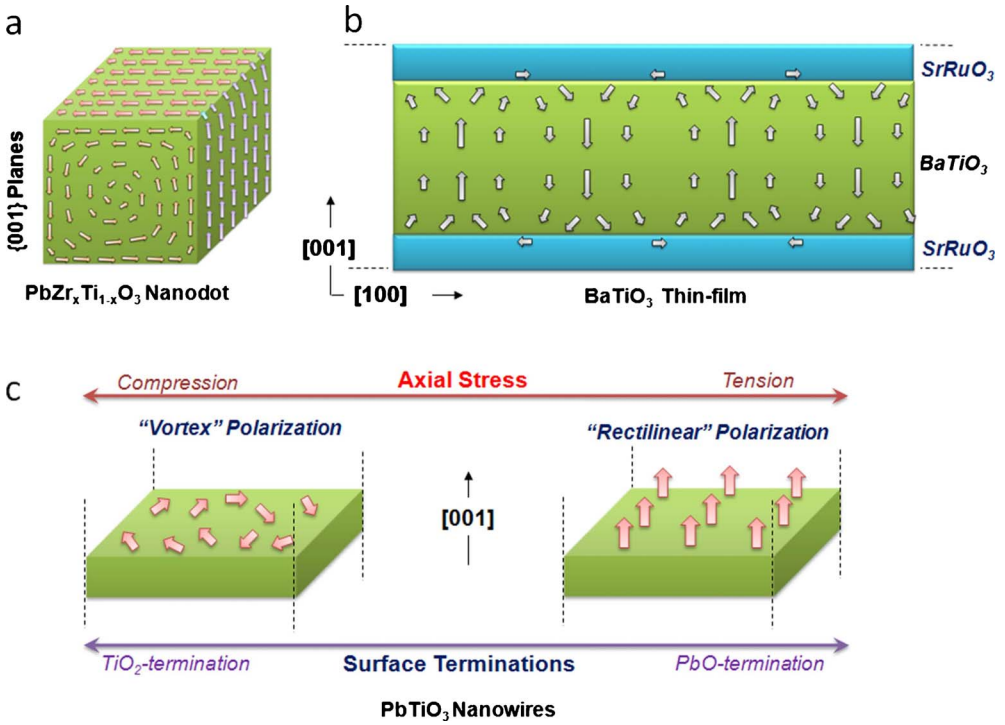

FIG. 1. (Color online) (a) Schematic view of nonrectilinear vortex polarization configuration in a 48 Å × 48 Å × 48 Å $PbZr_{0.4}Ti_{0.6}O_3$ nanodot as predicted by first-principles-based effective Hamiltonian techniques (based on Ref. 10). (b) DFT-predicted closure domain structure in ultrathin epitaxial $SrRuO_3/BaTiO_3/SrRuO_3$ ferroelectric capacitor (as reported in Ref. 14). (c) Influence of the axial strain and surface terminations on the favored nonrectilinear vortex and rectilinear axial polarization configurations in $PbTiO_3$ nanowires, based on the findings of the present work.

lateral (i.e., off-axis) polarization has in fact been observed at room temperature in single-crystal $BaTiO_3$ nanowires as small as 30 Å.[24,25] Although the presence of a vortex polarization state was not probed or ascertained in these prior efforts, recent DFT calculations support the simultaneous presence of nonzero lateral and a weak vortex polarization in TiO_2-terminated $BaTiO_3$ nanowires with a diameter of 16 Å.[20] A "strong" ferroelectric such as $PbTiO_3$ offers a testing ground to critically probe the manner in which polarization manifests under nanoscale one-dimensional boundary conditions.

In this contribution, we show based on parameter-free DFT computations that unambiguous nonrectilinear polarization configurations are indeed exhibited by ultrathin $PbTiO_3$ nanowires oriented along the [001] direction. Axial strain and nanowire sidewall terminations are shown to crucially determine whether the polarization occurs in axial rectilinear or vortex nonrectilinear forms. The interplay between the axial strain and sidewall terminations in determining the preferred polarization state is schematically illustrated in Fig. 1(c). In essence, at (or above) a critical size of 16 Å, TiO_2 sidewall terminations favor a vortex polarization state at equilibrium (characterized by a nonzero-axial toroidal moment and zero-axial polarization). However, PbO sidewall terminations favor the expected rectilinear axial polarization at equilibrium (characterized by a zero-axial toroidal moment and nonzero-axial polarization). Furthermore, regardless of the sidewall terminations, the vortex and axial polarization configurations are *mutually exclusive*, and are reversibly switchable from one to the other purely by the application of an axial stress. Below, we describe this discovery in greater detail.

II. METHODS AND MODELS

A. Computational details

Our zero-temperature calculations were performed within the local density approximation of density-functional theory[26] as implemented in the Vienna *ab initio* simulation package (VASP).[27] The electronic wave functions are expanded in plane waves up to a cut-off energy of 500 eV. The pseudopotentials based on the projector augmented wave method[28] explicitly include the O 2*s* and 2*p*, the Ti 3*s*, 3*p*, 3*d*, and 4*s*, and the Pb 5*d*, 6*s*, and 6*p* electrons in the valence states. We use a $1 \times 1 \times 6$ Monkhorst-Pack sampling of the Brillouin-zone integrations[29] for all nanowires. To obtain a geometry optimized equilibrium structure, atomic positions, and the *c* lattice parameter for each wire were fully relaxed using the conjugate gradient method until all the Hellmann-Feynman forces and the stress component were less than 0.02 V/Å and 1.0×10^{-2} GPa, respectively.

B. Model details

The initial geometries of the free standing, infinitely long and axially symmetric $PbTiO_3$ nanowires with axis along [001] were constructed by terminating bulk $PbTiO_3$ along the (100) and (010) lateral planes. We represent the nanowire

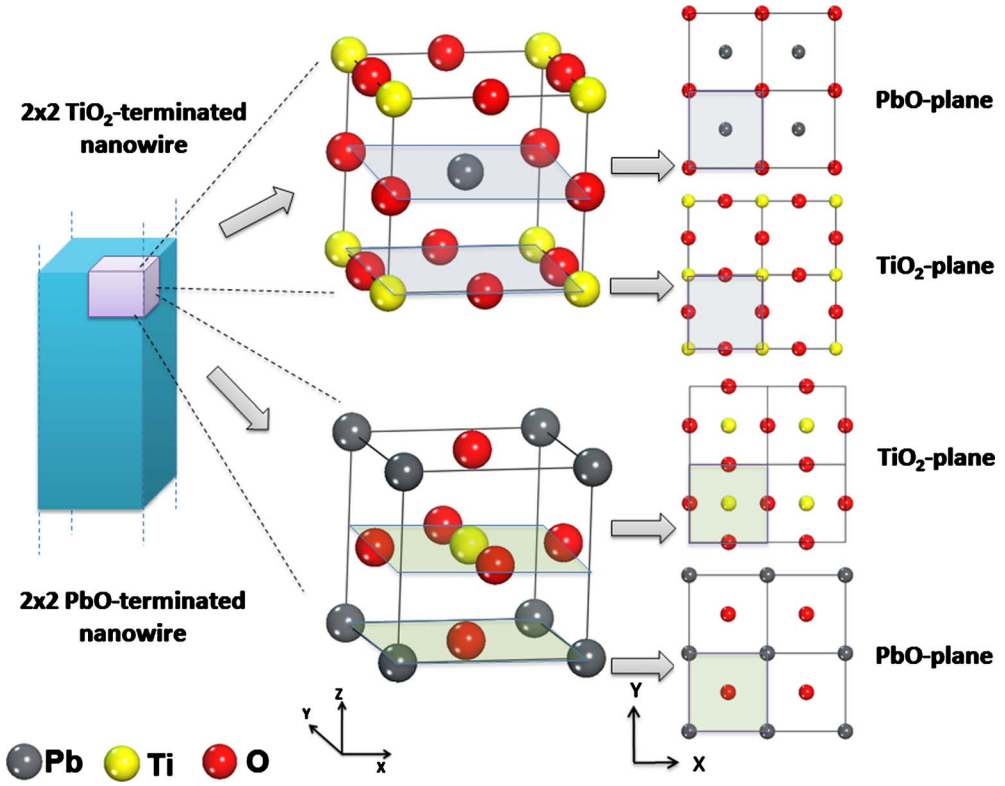

FIG. 2. (Color online) Schematic illustration showing construction of an infinitely long 2×2 nanowire with its axis along z direction. Either a Pb-centered (top) or a Ti-centered (bottom) perovskite unit cell can be used to construct the nanowire, which results in TiO_2- or PbO-terminated lateral sidewalls, respectively. The nanowire with either termination will display alternating layers of PbO and TiO_2 planes along the axial directions.

size by $n\times n$, where n is the number of $PbTiO_3$ unit cells along each of the x and y axes. Only nanowires with square cross sections and n varying from 1–4 were considered. Furthermore, all the sidewalls were assumed to be terminated either by PbO or TiO_2 planes. We also note that irrespective of the lateral termination all wires have an alternate stacking of PbO and TiO_2 planes along the axial direction. Figure 2 illustrates the nanowire construction for the specific case of the 2×2 nanowire.

For each nanowire, a reference paraelectric state was first considered. By imposing a mirror symmetry plane normal to the wire axis and passing through a TiO_2 layer, off center displacements of the Ti atoms were prevented. This axial constraint, combined with fourfold axisymmetric placement of all atoms at their respective bulk positions followed by point-group conserving geometry optimizations of the atomic coordinates, ensured that the final relaxed structure was in a purely paraelectric state. Starting from the relaxed paraelectric structure taken as a reference, we then searched for possible ferroelectric ground states for each nanowire. The mirror symmetry plane was removed by giving each Ti atom a small off-center displacement of $\sim$0.01 Å along the axial direction. We also imparted 1° clockwise (anticlockwise) displacements around the central nanowire axis on cations (anions) in the supercell to seed a vortex polarization instability in the system. Atomic positions of all the ions as well as the unit-cell vector along the nanowire axis were optimized.

C. Treatment of local polarization

Ferroelectric closure domains frequently pose a situation where a system shows no net polarization while still bearing a nonzero polarization locally. The Berry phase method[30,31] widely used to calculate net polarization does not carry site-specific, or local, information. Therefore, we use the positions and the bulk Born effective charges in the atoms to define a polarization vector within each unit cell as described below.

We introduce the local polarization per unit cell using the following equation:

$$\mathbf{p}_i = \frac{e}{\Omega_c}\sum_j w_{ji}\tilde{Z}_j^*\mathbf{u}_{ji}, \tag{1}$$

where index i runs over all the unit cells in the wire cross section and index j runs over all the atoms in a given unit cell. e, Ω_c, and $\mathbf{u}_{ji}$ denote electron charge, volume of the unit cell, and displacement of jth atom in ith unit cell in ferroelectric ground state with respect to a reference paraelectric state, respectively. $\tilde{Z}_j^*$ is the Born effective charge tensor of the cubic bulk $PbTiO_3$ for jth atom and w_{ji} is a weight factor. Weights are set to $w_{Pb}=1/8$, $w_{Ti}=1$, and $w_O=1/2$ for the PbO-terminated nanowires (assuming Ti centered unit cell) and $w_{Pb}=1$, $w_{Ti}=1/8$, and $w_O=1/2$ for the TiO_2-terminated nanowires (assuming Pb centered unit cell). For a given atom, the weight factor is determined by the inverse of the number of unit cells in the bulk that share the atom. In this

study, we have used the theoretical values of the Born effective charge tensors calculated by Zhong *et al.*[32] As a test of this method, the bulk polarization of the ferroelectric tetragonal phase of $PbTiO_3$ was computed to be 84.5 $\mu C/cm^2$, in good agreement with the value of 82 $\mu C/cm^2$ obtained using the Berry phase method[33] and the experimental value of 85 $\mu C/cm^2$ at room temperature[34] for the same phase. We note that the present approach of using Born effective charges to quantify local dipole moments has also been previously applied to study ferroelectric thin films and nanowires.[13,22,35,36]

Once the local polarization vectors are determined, one may define a toroidal moment, $g=\frac{1}{2Nv}\Sigma_i \mathbf{r}_i \times \mathbf{p}_i$, as has been done before.[37] Here, $\mathbf{p}_i$ is the dipole moment at the ith unit cell with the position vector $\mathbf{r}_i$ locating the center of the unit cell and N is the total number of unit cells, each with volume v. With these definitions, a given nanowire may, in general, possess a net nonzero polarization and a nonzero toroidal moment.

III. RESULTS

Our simulation results show that, in their stress-free ground state, $n \times n$ TiO_2-terminated nanowires for $n=1-3$ remain paraelectric and do not show any spontaneous polarization (axial or vortex). However, the ground state of the 4×4 TiO_2-terminated nanowire turns out to be a pure vortex state, which is 0.80 eV lower in energy with respect to the axially polarized nonvortex state. The local polarization vector forms a closed loop in the plane normal to the axis showing a zero net polarization along x, y, and z directions, and a nonzero moment of polarization along the axial direction. We thus predict that the critical size for the vortex polarization instability in TiO_2-terminated $PbTiO_3$ nanowire is about 16 Å. Figure 3 depicts the local dipoles for each unit cell (panel a) and displacements of the Pb, Ti, and the three inequivalent O atoms (panels b through f) with respect to the corresponding positions in the reference paraelectric state. The existence of the vortex state is clearly manifest (note the oppositely directed displacements for the cations and anions).

On the other hand, in their relaxed state, all four $n \times n$ PbO-terminated $PbTiO_3$ nanowires bear a significant axial polarization (listed in Table I), comparable to the bulk spontaneous polarization as predicted in the past,[22] but zero toroidal moment, despite the fact that intentional atomic displacements were imposed prior to geometry optimization to seed a vortex polarization configuration. The Table I contains the preferred polarization state and the optimal c lattice parameter along the axis at equilibrium for all nanowires considered. A clear correlation between the polarization state and c can be seen. For instance, the TiO_2-terminated nanowires display c values much smaller than the corresponding bulk value of 4.03 Å and hence axial polarization is entirely suppressed. A lateral critical size of 16 Å (corresponding to the 4×4 TiO_2-terminated nanowire which still has a small c value) appears to be sufficient to allow for the genesis of the vortex state. On the other hand, axial polarization (of about the same magnitude as in bulk) is favored in PbO-terminated nanowires as their c values are similar to the corresponding bulk value (albeit a little smaller). The presence of the axial polarization leaves little reason for the appearance of the vortex polarization state in these nanowires.

To understand the cause of the much reduced c lattice parameter (as compared to the bulk) in case of the relaxed TiO_2-terminated nanowires one should note that the ferroelectric instability in $PbTiO_3$ is strongly related to the covalent nature of the Pb-O bond. In other words, the stronger the covalency of the Pb-O bond the higher is the tetragonality. Based on their DFT calculations, Shimada *et al.*[22] have recently shown that in the $PbTiO_3$ nanowires (irrespective of the surface terminations) a charge transfer takes place from the interior of the wire to the surface upon relaxation to counter the coordinative unsaturations at the surface. In TiO_2-terminated wire, this charge transfer from the penultimate PbO layer to the outer TiO_2 layer decreases the covalency of Pb-O bonds and hence reduces the tetragonality. Furthermore, an increased charge density at the Ti-O bond centers at the surface further contracts the Ti-O bonds and therefore leads to a significantly smaller relaxed c lattice parameter as compared to the bulk. On the other hand, the same phenomenon helps the PbO-terminated nanowires to remain tetragonal with their c lattice parameter quite close to the bulk value.

To systematically study the effect of strain on axial polarization and toroidal moment, different levels of axial strain on all TiO_2- and PbO-terminated nanowires were imposed by constraining the c lattice parameter while allowing all other internal degrees of freedom to relax. The application of strains to the smallest three nanowires did not result in a drastic change in the manner of the polarization. For instance, compressive strains maintained the 1×1, 2×2, and 3×3 TiO_2-terminated nanowires in the paraelectric state and tensile strains resulted in the gradual appearance of an axial polarization. Likewise, tensile, and compressive strains resulted in slight increases and decreases, respectively, in axial polarization in the 1×1, 2×2 and 3×3 PbO-terminated nanowires.

However, the 4×4 TiO_2- and PbO-terminated nanowires responded quite differently to strain. The behavior of the 4×4 TiO_2- and 4×4 PbO-terminated nanowires as a function of axial strain is captured in Fig. 4. It can be seen that in both cases, axial strain of the correct sign and magnitude can cause a phase transition between the pure vortex and pure axial polarization states. For instance, while the 4×4 PbO-terminated (TiO_2-terminated) nanowire adopts a rectilinear axial (nonrectilinear vortex) polarization state at equilibrium, an axial compressive (tensile) stress of about −3.5% (3%) results in the onset of an abrupt phase transition to a pure vortex (pure axial) polarization state. That the polarization state of a PbO-terminated 4×4 nanowire under 3.5% compressive strain is indeed of the vortex type is established by the local dipole moments (panel g) and atomic displacements (panels h–l) shown in Fig. 3(b). We also make an interesting observation that the transition between vortex and axial polarization states occurs at exactly the same value for the c lattice parameter (3.87 Å) along the nanowire axis for the both types of $PbTiO_3$ nanowires. It thus appears that the c value determines the nature of polarization state. Since the c

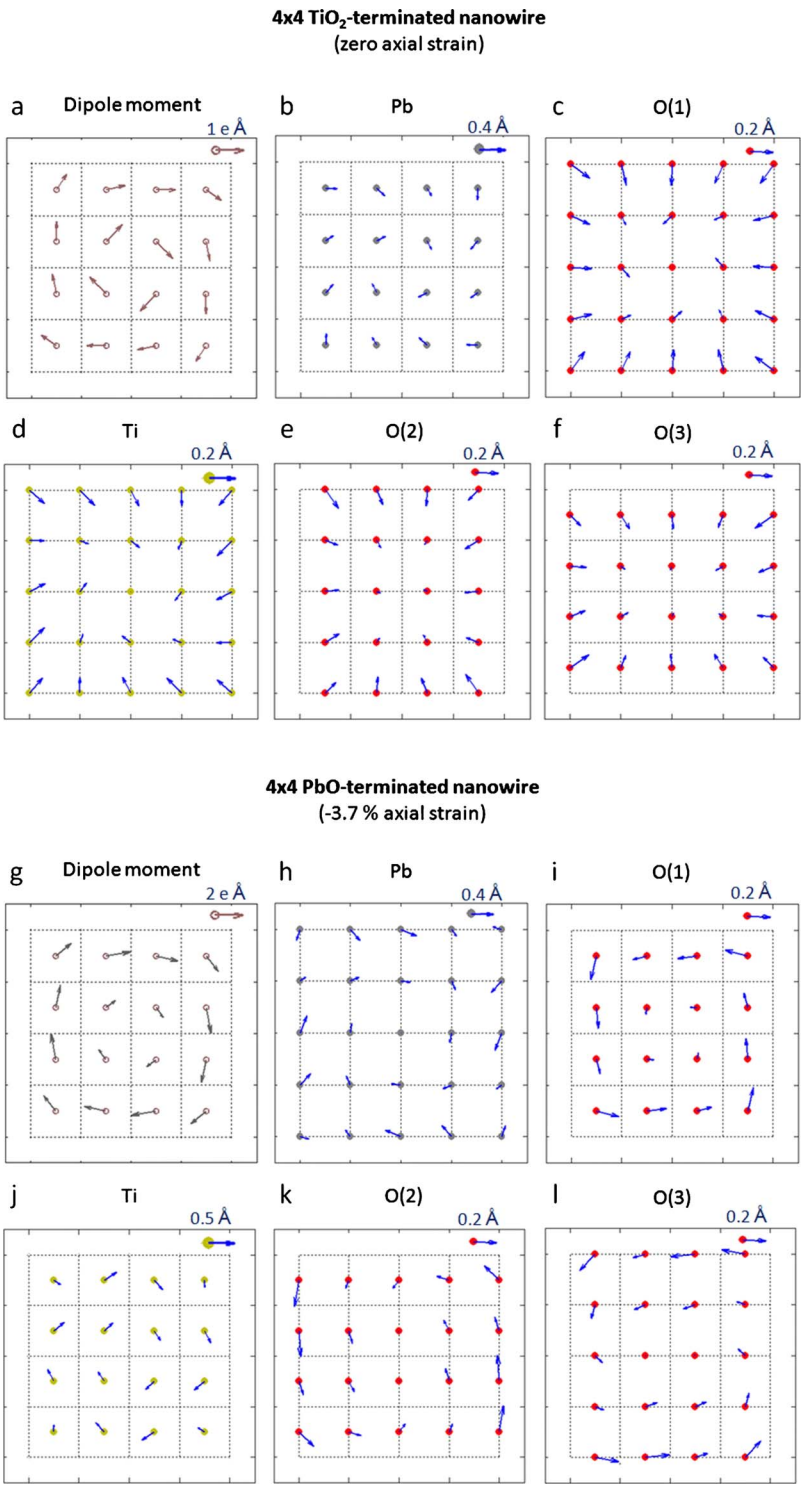

FIG. 3. (Color online) Unit-cell-decomposed dipole moments (panel a) and in-plane displacements of individual atoms with respect to a paraelectric reference state in PbO (panels b and c) and TiO_2 (panels d–f) transverse planes for a 4×4 TiO_2-terminated nanowire at zero axial strain. Panels g–l, same as panels a–f, but for a 4×4 PbO-terminated nanowire at 3.7% axial compressive strain. Dotted lines represent the boundary of each individual unit cell in the wire cross section.

value for a given nanowire is determined by both intrinsic and extrinsic factors such as strain, sidewall terminations and passivation, these factors can be used to control the polarization state of the system. In order to assess the validity of using the stress-free bulk Born effective charges in the determination of the local dipole moments and the polarization, we have calculated the axial polarization of both the 4×4 PbO- and the 4×4 TiO_2-terminated nanowires for a few choices of strains by employing actual Born effective charges (calculated for the corresponding nanowires through density functional perturbation theory). These results are displayed in Fig. 4, and as can be seen, the two approaches yield results within about 10% of each other

We now briefly compare the nature of the ferroelectric instabilities in $PbTiO_3$ nanowires with those in $BaTiO_3$ nanowires.[20] Despite different intrinsic tendencies toward ferroelectricity in the corresponding bulk systems, our *ab initio* studies on $BaTiO_3$ and $PbTiO_3$ nanowires predict the same critical size (i.e., 4×4 unit cells in the wire cross section) and termination (i.e., the TiO_2 termination) for the ap-

TABLE I. Polarization states and c lattice parameters at equilibrium for each of the four PbO- and TiO_2-terminated nanowires discussed in this work. The bulk results are also provided for comparison. "P" and "F" represent the paraelectric and ferroelectric ground states, respectively. In case of the ferroelectric ground state, the preferred polarization configuration is also indicated in parenthesis for the nanowires. The net axial polarizations for PbO-terminated nanowires are also listed.

	Nanowire size				
	1×1	2×2	3×3	4×4	Bulk
			TiO_2-terminated		
Ground state	P	P	P	F (vortex)	F
c(Å)	3.39	3.57	3.68	3.76	4.03
			PbO-terminated		
Ground state	F (axial)	F (axial)	F (axial)	F (axial)	F
Axial polarization ($\mu C/cm^2$)	103.05	100.34	92.93	90.53	84.50
c(Å)	3.92	3.97	3.99	4.01	4.03

pearance of the vortex type instability in these two systems. Still, there are some differences to note as well. First, owing to their strong intrinsic tendency for ferroelectric polarization, $PbTiO_3$ nanowires show significantly enhanced vortex type instability compared to $BaTiO_3$ nanowires. Second, unlike $PbTiO_3$ nanowires, $BaTiO_3$ nanowires (because of the preferred axis of polarization being along [111]) also display a nonzero off-axis component of the polarization. Thus, while the axial and vortex polarization states are mutually exclusive in the case of $PbTiO_3$ nanowires, this is not the case in $BaTiO_3$ nanowires.

In order to further clarify the nature of the "vortex polarization instability," we carried out zone center phonon mode analysis for the 4×4 TiO_2-terminated nanowire with zero axial strain and the 4×4 PbO-terminated wire at −3.7% (i.e., compressive) axial strain in their respective reference paraelectric states. Any imaginary frequencies obtained in such analyses should correspond to possible instabilities of the paraelectric system. Imaginary frequencies were indeed found for both cases, with eigenvectors corresponding to a vortex type of distortion of the reference paraelectric state. As the $3N$ mode eigenvectors (ϕ_is) of an N-atom system form a complete and orthonormal set of distortions, any arbitrary distortion of the system can be decomposed as a linear combination of these $3N$ mode eigenvectors. Here, we decompose a vector ψ representing the displacements of the atoms in the vortex state of polarization with respect to the

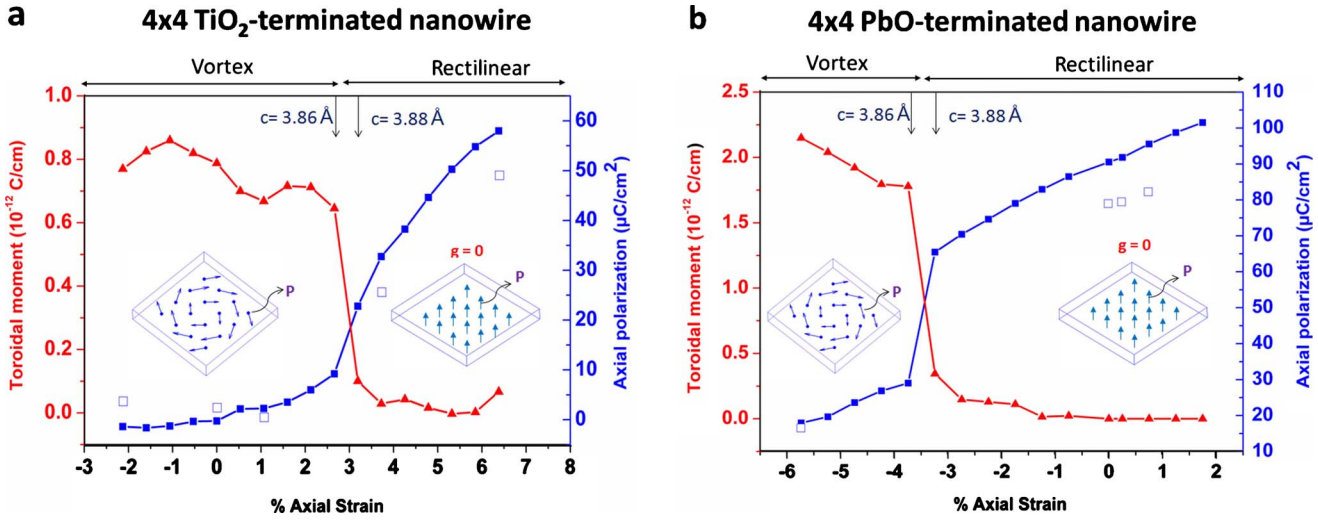

FIG. 4. (Color online) (a) Toroidal moment [gray (red) triangles, using the left axis] and axial polarization [black (blue) solid squares, using the right axis] as a function of axial strain for the 4×4 TiO_2-terminated nanowire. Black (blue) hollow squares represent values of axial polarization calculated using actual Born effective charges (obtained through density functional perturbation theory) instead of the bulk Born effective charges. In its relaxed state (zero-axial strain) the nanowire bears a significant amount of toroidal moment (0.79×10^{-12} C/cm) with negligible axial polarization. Application of axial tensile strain of about 3% leads to a switching from the vortex to the axial-polarized state (shown in inset). (b) Same as (a), but for the 4×4 PbO-terminated nanowire. The relaxed state of the nanowire is axially polarized with zero toroidal moment, however a compressive axial strain of about 3.5% leads to a phase transition from the axial to a vortex polarized state. The phase transition in both nanowires occur abruptly at a c value of 3.87 Å, as indicated in a and b.

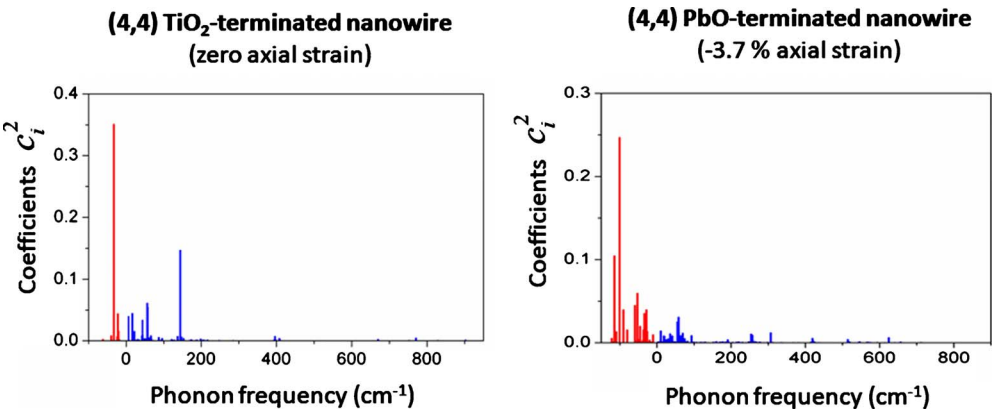

FIG. 5. (Color online) Plot of coefficients $|C_i|^2$ against phonon mode frequencies, obtained by zone center phonon mode analysis of the reference paraelectric states, for the relaxed 4×4 TiO_2-terminated nanowire (left) and the 4×4 PbO-terminated nanowire at 3.7% axial compressive strain (right). Imaginary and real frequencies are plotted in gray (red) and black (blue) on negative and positive x axis, respectively.

appropriate reference paraelectric state, in terms of the mode eigenvectors as described below.

We define a displacement vector ψ as

$$\psi = \begin{pmatrix} \Delta_x^1 \\ \Delta_y^1 \\ \Delta_z^1 \\ \Delta_x^2 \\ \Delta_y^2 \\ \Delta_z^2 \\ \vdots \end{pmatrix}, \tag{2}$$

where Δ_α^τ is the relative displacement of atom τ along Cartesian direction $\alpha(=x,y,z)$ in the vortex polarization state with respect to the reference paraelectric state. The normalized displacement vector $\psi_n(=\psi/|\psi|)$ can then be expressed as a linear combination of zone-center phonon mode eigenvectors of the reference paraelectric state, as follows:

$$\psi_n = \sum_{i=1}^{3N} C_i \phi_i, \tag{3}$$

where C_i are scalar coefficients calculated using the orthonormality of $\phi_i s$, i.e., $C_i = \langle \phi_i | \psi_n \rangle$. The square of coefficients $C_i s$ are plotted against vibrational frequencies corresponding to the mode eigenvectors in Fig. 5. We note that large contributions to the vortex distortion indeed come from vibrational eigenmodes with imaginary frequencies (plotted in red on the negative frequency axis of Fig. 5) with the largest contribution corresponding to a vortex distortion of the reference paraelectric state. This instability is analogous to the soft-mode distortions seen in bulk ferroelectric materials that display spontaneous rectilinear polarization.

IV. SUMMARY

Our parameter-free DFT calculations demonstrate the existence of novel electric dipole polarization ordering, and the possibility of polarization switching, in $PbTiO_3$ nanowires. The choice of $PbTiO_3$ is motivated by its strong intrinsic tendency for polarization. Rectilinear axial and nonrectilinear vortex polarization ordering occur in these nanowires in a mutually exclusive manner, and switching between these polarization states may be accomplished through axial stress (and perhaps other extrinsic factors not explored here). The vortex polarization instability is characterized by local polarization vectors curling in the plane normal to the nanowire axis with a purely axial first moment of the polarization. We predict that the critical size for the genesis of the vortex state in $PbTiO_3$ nanowires is 16 Å at zero temperature. At higher temperatures, nanowires with larger diameters may be required to support the vortex polarization state. Control of such exotic polarization states in low-dimensional systems offer transformative technological possibilities. We hope that our computational results will motivate experimental efforts in these directions.

ACKNOWLEDGMENTS

This material is based upon work supported by the Office of Naval Research. Computational support was provided through a National Science Foundation Teragrid Resource Allocation.

*rampi@ims.uconn.edu

[1] L. E. Cross, *Ferroelectric Ceramics*, edited by N. Setter and E. L. Colla (Birkhäuser Verlag, Basel, 1993), pp. 1–85.
[2] *Physics of Ferroelectrics: A Modern Perspective*, edited by K. Rabe, Ch. H. Ahn, and J.-M. Triscone (Springer-Verlag, Berlin, 2007).
[3] J. F. Scott, Science **315**, 954 (2007).
[4] W. Lee, H. Han, A. Lotnyk, M. A. Schubert, S. Senz, M. Alexe, D. Hesse, S. Baik, and U. Gösele, Nat. Nanotechnol. **3**, 402 (2008).
[5] P. R. Evans, X. Zhu, P. Baxter, M. McMillen, J. McPhillips, F. D. Morrison, J. F. Scott, R. J. Pollard, R. M. Bowman, and J. M. Gregg, Nano Lett. **7**, 1134 (2007).
[6] Z. Hu, M. Tian, B. Nysten, and A. M. Jonas, Nature Mater. **8**, 62 (2009).
[7] C. Kittel, Phys. Rev. **70**, 965 (1946).
[8] R. J. Harrison, R. E. Dunin-Borkowski, and A. Putnis, Proc. Natl. Acad. Sci. U.S.A. **99**, 16556 (2002).
[9] I. I. Naumov, L. Bellaiche, and H. X. Fu, Nature (London) **432**, 737 (2004).
[10] S. Prosandeev and L. Bellaiche, Phys. Rev. B **75**, 094102 (2007).
[11] I. Ponomareva, I. I. Naumov, and L. Bellaiche, Phys. Rev. B **72**, 214118 (2005).
[12] J. Wang, M. Kamlah, and T.-Y. Zhang, J. Appl. Phys. **105**, 014104 (2009).
[13] T. Shimada, S. Tomoda, and T. Kitamura, Phys. Rev. B **81**, 144116 (2010).
[14] P. Aguado-Puente and J. Junquera, Phys. Rev. Lett. **100**, 177601 (2008).
[15] M. K. Roy, S. Sarkar, and S. Dattagupta, Appl. Phys. Lett. **95**, 192905 (2009).
[16] B. J. Rodriguez, X. S. Gao, L. F. Liu, W. Lee, I. I. Naumov, A. M. Bratkovsky, D. Hesse, and M. Alexe, Nano Lett. **9**, 1127 (2009).
[17] A. Gruverman, D. Wu, H.-J. Fan, I. Vrejoiu, M. Alexe, R. J. Harrison, and J. F. Scott, J. Phys.: Condens. Matter **20**, 342201 (2008).
[18] X. H. Zhu, P. R. Evans, D. Byrne, A. Schilling, R. Douglas, J. Pollard, R. M. Bowman, J. M. Gregg, F. D. Morrison, and J. F. Scott, Appl. Phys. Lett. **89**, 122913 (2006).
[19] C. Thompson, D. D. Fong, R. V. Wang, F. Jiang, S. K. Streiffer, K. Latifi, J. A. Eastman, P. H. Fuoss, and G. B. Stephenson, Appl. Phys. Lett. **93**, 182901 (2008).
[20] G. Pilania, S. P. Alpay, and R. Ramprasad, Phys. Rev. B **80**, 014113 (2009).
[21] G. Geneste, E. Bousquet, J. Junquera, and P. Ghosez, Appl. Phys. Lett. **88**, 112906 (2006).
[22] T. Shimada, S. Tomoda, and T. Kitamura, Phys. Rev. B **79**, 024102 (2009).
[23] J. Hong, G. Catalan, D. N. Fang, E. Artacho, and J. F. Scott, Phys. Rev. B **81**, 172101 (2010).
[24] W. S. Yun, J. J. Urban, Q. Gu, and H. Park, Nano Lett. **2**, 447 (2002).
[25] J. E. Spanier, A. Kolpak, I. Grinberg, J. J. Urban, L. Ouyang, W. S. Yun, A. M. Rappe, and H. Park, Nano Lett. **6**, 735 (2006).
[26] R. Martin, *Electronic Structure: Basic Theory and Practical Methods* (Cambridge University Press, New York, 2004).
[27] G. Kresse and J. Furthmüller, Phys. Rev. B **54**, 11169 (1996).
[28] P. E. Blöchl, Phys. Rev. B **50**, 17953 (1994).
[29] H. J. Monkhorst and J. D. Pack, Phys. Rev. B **13**, 5188 (1976).
[30] R. D. King-Smith and D. Vanderbilt, Phys. Rev. B **47**, 1651 (1993).
[31] R. Resta, Rev. Mod. Phys. **66**, 899 (1994).
[32] W. Zhong, R. D. King-Smith, and D. Vanderbilt, Phys. Rev. Lett. **72**, 3618 (1994).
[33] Y. Duan, H. Shi, and L. Qin, J. Phys.: Condens. Matter **20**, 175210 (2008).
[34] R. J. Nelmes and W. F. Kuhs, Solid State Commun. **54**, 721 (1985).
[35] B. Meyer and D. Vanderbilt, Phys. Rev. B **65**, 104111 (2002).
[36] T. Shimada, Y. Umeno, and T. Kitamura, Phys. Rev. B **77**, 094105 (2008).
[37] S. Prosandeev, I. Kornev, and L. Bellaiche, Phys. Rev. B **76**, 012101 (2007).